Journal of Luminescence 255 (2023) 119600

Contents lists available at ScienceDirect

Journal of Luminescence

journal homepage: www.elsevier.com/locate/jlumin

Full Length Article

Enhanced radioluminescence and improved radioluminescent nuclear battery output performance more than 50% with SiO_2 nanosphere coating

Yuhang He [a], Zhiheng Xu [a,b,*], Hongyu Wang [a], Mingxin Bian [a], Yunpeng Liu [a,b], Xiaobin Tang [a,b,**]

[a] Department of Nuclear Science and Technology, Nanjing University of Aeronautics and Astronautics, Nanjing, 211106, China
[b] Key Laboratory of Nuclear Technology Application and Radiation Protection in Astronautics, Ministry of Industry and Information Technology, Nanjing, 211106, China

ARTICLE INFO

Keywords:
Radioluminescent nuclear battery
SiO_2 nanosphere coating
Electrical output performance enhancement
Radioluminescent intensity

ABSTRACT

Radioluminescent nuclear battery as a typical representative of small power device based on the generation and utilization of radioluminescence, which can stable energy supply for equipment in extreme environments. To date, the development of such nuclear battery is primarily limited by the weak radioluminescence intensity. In this work, a method of adding SiO_2 nanosphere coating to the fluorescent layer is proposed to solve the problem of weak radioluminescence and significantly improve the battery's output performance. The SiO_2 nanosphere coating can promote the radiative transition rate and quantum efficiency of the ZnS:Cu phosphor of fluorescent layer and the radioluminescent intensity of the ZnS:Cu fluorescent layer increases by 62.32%. And the maximum output power of the corresponding radioluminescent nuclear battery is enhanced by 51.59% compared with that before optimization, under the same X-ray excitation condition.

1. Introduction

As a kind of energy supply device with the advantages of long life and stable output, the nuclear battery can provide energy for space equipment such as satellites and detectors in extreme environments such as deep space [1,2]. Radioluminescent nuclear battery (RLNB), as a typical representative of small nuclear battery, shows great potential to provide energy support for aerospace devices in future space exploration [3]. As shown in Fig. 1, the RLNB can be divided into three main parts: radioactive sources, fluorescent layer, and photovoltaic (PV) modules. The fluorescent layer of the RLNB can convert decay energy from radioactive sources into light energy. Then the PV module converts the light energy into electrical output through the photoelectric effect [4]. And the output performance of the nuclear battery based on indirect energy conversion is much higher than the nuclear battery which converts decay directly into electric energy [5]. The fluorescent layer as the most important part of the RLNB not only protects the PV modules from radiation damage [6,7] and increases the service life [8,9], but also affects the output performance of the battery. For example, the radioluminescence intensity of the fluorescent layer or the coupling between the response range of the PV module and the spectral range of radioluminescence can determine the electrical output performance of the battery [10,11]. Based on this, it is necessary to take effective measures to enhance the radioluminescence intensity or modulate spectral range of the fluorescent layer, to improve the output performance and expand the application scenarios of the battery [12–15].

Many optimization methods for increasing the radioluminescence properties of the fluorescent layer and improving the output performance of the RLNB have been proposed. These methods can be divided into two main categories, one of which is using new fluorescent materials with good properties. Xu et al. [16,17] proposed a method that prepare a fluorescent layer of perovskite nanocrystals, which can freely adjust emission wavelength. The radioluminescence spectral range of this fluorescent layer matches the response interval of photovoltaic modules better, thus improving the electric output performance of the battery. And Li et al. [18] doped Mn^{2+} in $Cs_3Cu_2I_5$ and prepared it as a fluorescent layer to improve the output performance of the RLNB as well as the irradiation stability. Another method is to use existing materials with good luminous properties to improve their radioluminescence intensity through various methods. For example, ZnS:Cu is a fluorescent material that produces yellow-green light with excellent optical properties, energy conversion rate and irradiation resistance [19–21].

* Corresponding author. Department of Nuclear Science and Technology, Nanjing University of Aeronautics and Astronautics, Nanjing, 211106, China
** Corresponding author. Department of Nuclear Science and Technology, Nanjing University of Aeronautics and Astronautics, Nanjing, 211106, China
E-mail addresses: xuzhiheng@nuaa.edu.cn (Z. Xu), tangxiaobin@nuaa.edu.cn (X. Tang).

https://doi.org/10.1016/j.jlumin.2022.119600
Received 22 September 2022; Received in revised form 22 November 2022; Accepted 5 December 2022
Available online 8 December 2022

Extensive studies have been carried out for radioluminescent nuclear battery prepared from this fluorescent material [22–24]. Jiang et al. [25] proposed a method for irradiation modification of ZnS:Cu phosphor to improve the radioluminescent performance. However, this method is difficult to operate and will change the structure of the material. And Zhang et al. [26] proposed a method of using Al film as a visible light reflector on ZnS:Cu fluorescent layer. This method not only does not change the structure of the material itself but also increases the maximum output of the battery by 34.22%. On the basis of these enhancement methods, we propose a method to enhance the radioluminescence properties of the ZnS:Cu fluorescent material without changing its properties and structures.

Specifically, we add SiO_2 nanosphere coating to the fluorescent layer by gravitational deposition method and spin-coating process. This method successfully enhances the radioluminescence performance of ZnS:Cu fluorescent layer by enhancing the quantum efficiency of fluorescent materials and improves the electrical output performance of the RLNB without changing the properties and structure of the material. And the structure of the fluorescent layer in this work has a much more significant improvement in the RLNB output performance than the current fluorescent layer structure.

2. Materials and method

2.1. Preparation of fluorescent layer with SiO_2 nanosphere coating

Approximately 3.5 mL of ammonia (25%, AR) and 1.5 mL of deionized water are mixed and heated to 303 K and 25 mL of anhydrous ethanol (99.7%, AR) and 2.4 mL of tetraethyl orthosilicate (99%, GC) are mixed and sonicate for 30 min, then add to the deionized water mixture and stir at 303 K for 12 h. The precipitate is obtained by centrifugal separation and drying. The SiO_2 powders are ultrasonically dispersed in anhydrous ethanol at 2 wt%. The glass substrate is placed vertically into the solution, then place in a blast drying oven and dry for 3 h for preparation of the SiO_2 nanosphere coating.

Polystyrene and xylene (99%, AR) are mixed in the ratio of 1 g:2.5 mL and stirred for 12 h for the preparation of a transparent liquid. The ZnS:Cu phosphors (Purchased from Guangzhou Chuang Rong Chemical Technology Co, particle size of 15 μm) and the prepared solution are mixed according to the mass ratio of 1:1 and use the magnetic mixer to mix it fully for 30 min. The mixture dropwise on the SiO_2 nanosphere coating and spin-coating for 5 s at a speed of 1000 rpm to cover the surface of the coating. Then the fluorescent layer is cured by spin-coating at 5000 rpm for 90 s. And the fluorescent layers without SiO_2 nanosphere coating are prepared by dropping the mixture directly onto the glass substrate and using the same spin-coating process.

2.2. FDTD simulations of fluorescence enhancement

The simulation is performed using the Finite Difference Time Domain (FDTD) method. The emission process of ZnS:Cu is simulated using an electric dipole set at the coordinates of (0, 0, 0) μm with a wavelength range of 400–650 nm and the emission direction along the z axis. At a distance of 15 nm from the dipole, random distribution of SiO_2 nanospheres with a diameter of 450 nm is set up, where the center coordinate of the centermost SiO_2 nanosphere is (0, 0, −0.24) μm. And a perfectly matched layer (PML) is used at the x, y and z boundaries of the SiO_2 nanospheres to absorb the light. An electric field monitor is placed at z = 0 μm to analyze the electric field distribution of the fluorescence emission process. A power monitor analysis group with center coordinates at (0, 0, −0.2) μm and span of 0.6 μm is set up to obtain the output power when the output electric dipole interacts with SiO_2. A smaller power monitor analysis group set with span of 0.015 μm and centered at (0, 0, 0) μm is set to obtain the output power of the electric dipole alone.

The change of quantum efficiency η after adding SiO_2 nanospheres is calculated using the method described in references [27–30].

$$\eta = \frac{\Gamma_{rad}}{(\Gamma_{tot} + (1 - \eta_i)/\eta_i)} \tag{1}$$

$$\Gamma_{rad} = P_{rad}/P_0 \tag{2}$$

$$\Gamma_{tot} = P_{tot}/P_0 \tag{3}$$

where Γ_{rad} represents radiative decay rate, Γ_{tot} represents total decay rate, and η_i represents initial quantum efficiency (which is set to 13.3% in this work [31]).

2.3. Optical and electrical properties testing

An electron-multiplying charge-coupled devices (ECCD) camera (Andor iXon Ultra 888, USA) equipped with a Canon EF 24–70 mm f/2.8L II USM zoom lens is used to record the images of the fluorescent layer. This work uses the X-ray to excite fluorescent materials to produce radioluminescence, and the voltage and current of the X-ray tube mainly control its intensity. The specific test environment as shown in Fig. 2. The ZnS:Cu fluorescence layer is located directly in front of the X-ray tube gate, and the lens of the ECCD camera is pointed at the fluorescence layer. When the ZnS:Cu material is excited by the X-ray, the radioluminescent photons emitted from the surface of the fluorescence layer are captured by the ECCD camera. And the radioluminescence spectra is obtained by Agilent Technologies Cary Eclipse fluorescence spectrophotometer. The images taken by the ECCD camera can be processed by ImageJ software to obtain the intensity of the radioluminescence photons generated on the surface of different fluorescent layers.

Based on the previous work about RLNB preparation and performance optimization, AlGaInP-based PV modules are chosen in this work. And the AlGaInP-based PV modules show good photovoltaic conversion performance and have a good matching with radioluminescence spectroscopy of ZnS:Cu. On this basis, we explore the enhancement

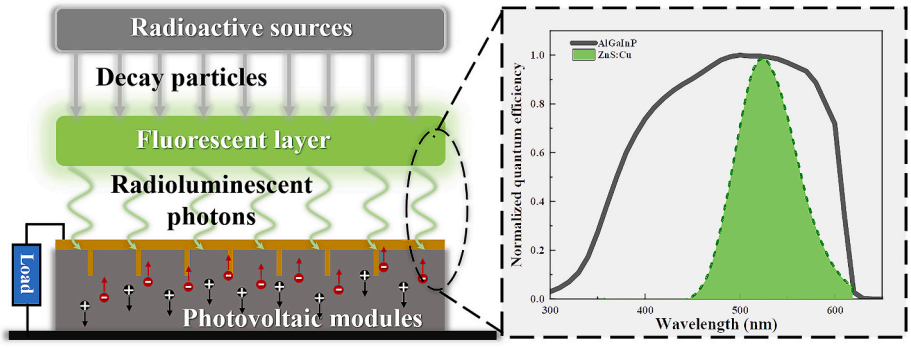

Fig. 1. Working mechanism of the radioluminescent nuclear battery.

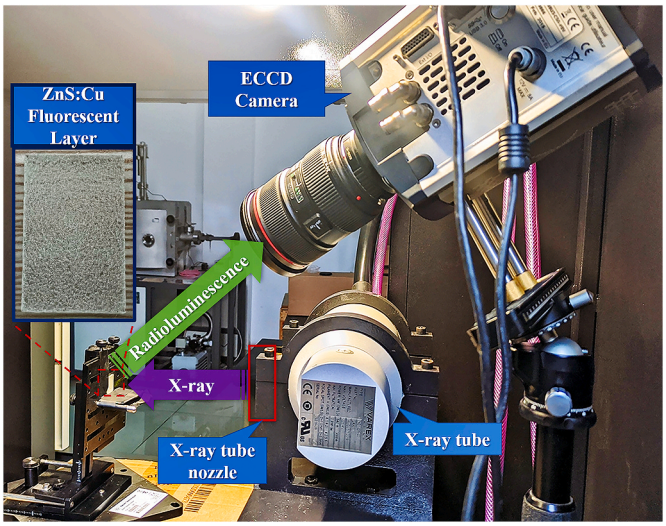

Fig. 2. Testing environment of photons intensity on the surface of fluorescent layer.

mechanism of fluorescent layer, and compare its effect with different optimization methods. The electrical property of the RLNB is evaluated by the Keithley 2636A source meter.

3. Results and discussion

3.1. Structural characterization

Fig. 3 shows the SEM images of the ZnS:Cu fluorescent layer and SiO_2 nanosphere coating. From the image of the cross-section of the prepared ZnS:Cu fluorescent layer, the structure of fluorescent layer is divided into three parts: glass substrate, SiO_2 nanosphere coating and ZnS:Cu phosphor layer. The ZnS:Cu phosphor layer and SiO_2 nanosphere coating are just closely adhered to each other, and do not change the structure of the ZnS:Cu phosphor. The thickness of the SiO_2 nanosphere coating is about 80 μm and the SiO_2 nanospheres in the coating are randomly distributed. In addition, the glass substrate only plays a supporting role so other materials can replace it according to the actual situation.

Fig. 4a shows the average particle size of the SiO_2 nanosphere particles is 450 nm in the coating. The photoluminescence (PL) spectrum of the ZnS:Cu (excited by the 300 nm UV) and the reflection spectrum of SiO_2 nanosphere coating prepared in this work, as shown in Fig. 4b. The ZnS:Cu has one emission peak centered at 518 nm and these two spectra have a large overlap from 400 to 600 nm, which is beneficial for the interaction of the ZnS:Cu and SiO_2 nanospheres coating.

3.2. Radioluminescence analysis

The radioluminescence properties of the fluorescent layers prepared in this work under different X-ray excitation conditions are further analyzed. Fig. 5 represents the ECCD camera recorded images of radioluminescent photons emitted from the surface of fluorescent layers under the X-ray with different voltages of X-ray tube (40 kV, 50 kV, 60 kV) and the current of X-ray tube is kept at 0.8 mA. And the SiO_2 nanosphere coating is added to the fluorescent layer in Fig. 5b. When the ZnS:Cu fluorescent layer is not excited, almost no radioluminescent photons are produced. However, when it is excited by the X-ray, a large number of radioluminescent photons are produced on the surface. The number of photons from the fluorescence layer with SiO_2 nanosphere coating is more than the fluorescence layer without SiO_2 nanosphere coating in the same situation. They all increase with the increase of the voltage of the X-ray tube.

Fig. 6a shows the variation of the radioluminescent photon intensity produced by fluorescent layers varied with the X-ray intensity. It can be seen that the radioluminescent photon intensity produced by the fluorescent layer increases with the X-ray intensity. And under the same excitation conditions, the photon intensity of ZnS:Cu fluorescent layer with SiO_2 nanosphere coating is greater than fluorescent layer without coating. The radioluminescence spectra of the fluorescent layer excited by X-ray is measured when the voltage of X-ray tube is 60 kV and the current of X-ray tube is 0.8 mA, as shown in Fig. 6b. Under the excitation of X-rays, the emission peak of ZnS:Cu is concentrated at 526 nm. The SiO_2 nanosphere coating does not emit fluorescence under X-ray excitation and does not affect the peak position of the ZnS:Cu radioluminescence spectrum. Thus, adding it to the fluorescent layer serves to increase the radioluminescence intensity and does not significantly affect the luminous properties of the ZnS:Cu fluorescent material itself. Moreover, when the voltage of the X-ray tube reaches 60 kV, the radioluminescence intensity of the fluorescent layer increases by 62.32% with the addition of SiO_2 nanosphere coating.

3.3. Enhancement mechanism analysis of radioluminescence

The model is established in FDTD based on the experimental results, as shown in Fig. 7. It contains randomly distributed SiO_2 nanospheres and a dipole is located directly above them. The luminescence phenomena and process of radioluminescence and photoluminescence are similar and both generate electron-hole pairs. Electron-hole pair composite and de-excitation produce radioluminescence [32]. Therefore, dipoles are used instead of electron-hole pairs in this work to simulate the radioluminescence process [33].

As shown in Fig. 8a, the electric field intensity gradually decreases from the inside to the outside and uniformly distributed, for the case of only dipole. Fig. 8b describes the field intensity of dipole with SiO_2 nanospheres. The fluorescence resonance between SiO_2 nanospheres and dipoles changes the electric field distribution. So the distribution range of the electric field becomes larger, from regular circular to

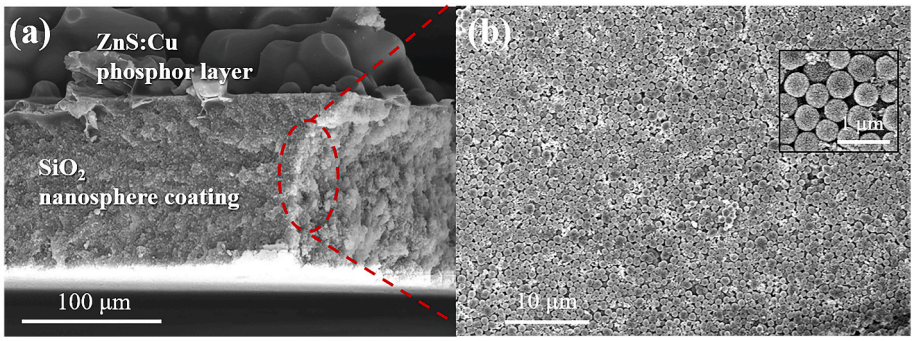

Fig. 3. SEM characterization images of the cross-section of (a) the prepared ZnS:Cu fluorescent layer and (b) the surface of the prepared SiO_2 nanosphere coating.

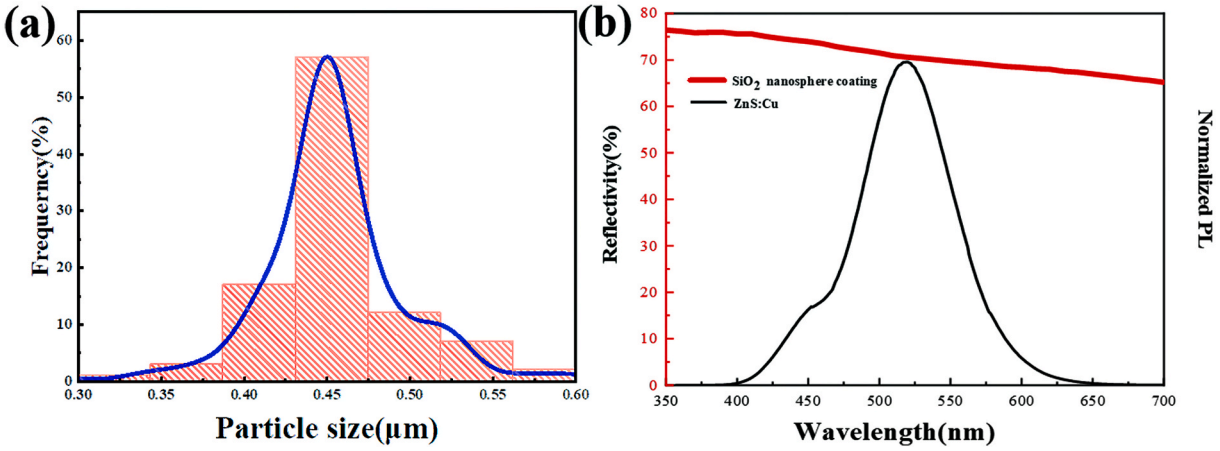

Fig. 4. (a) Particle size distribution of SiO_2 nanospheres. (b) The reflection spectrum of SiO_2 nanosphere coating and normalized PL spectrum of the ZnS:Cu.

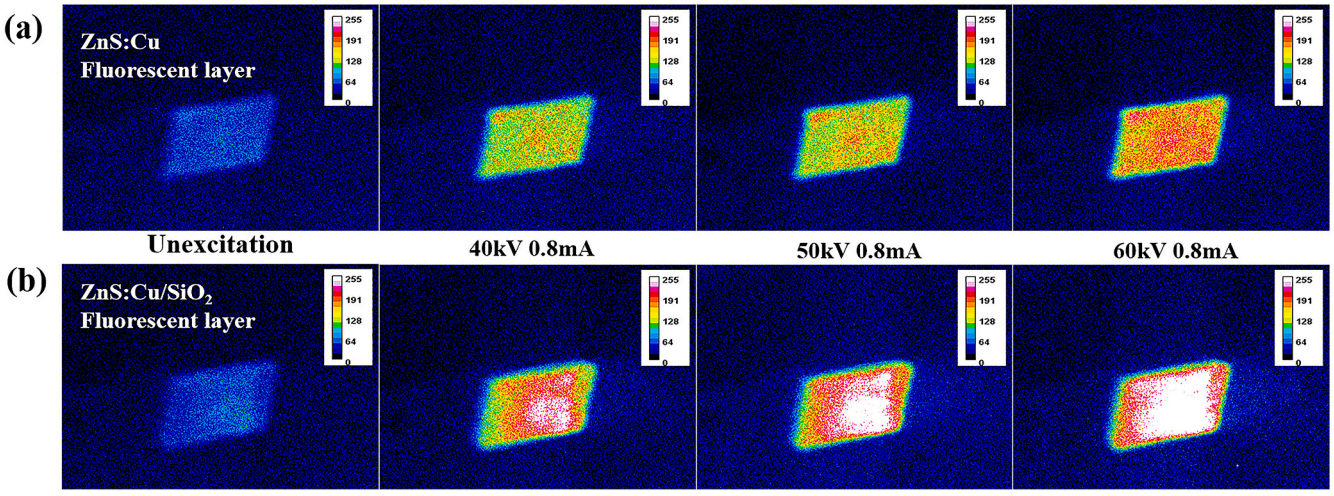

Fig. 5. Radioluminescent images of ZnS:Cu fluorescent layers (a) without SiO_2 nanosphere coating and (b) with SiO_2 nanosphere coating under different X-ray excitation conditions.

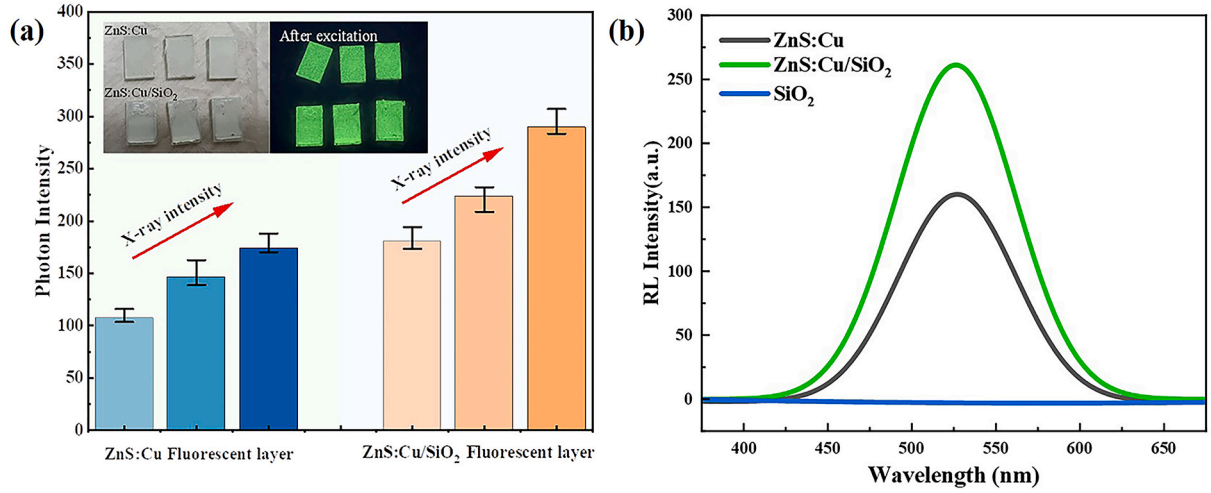

Fig. 6. (a) The radioluminescent photon intensity of fluorescent layers under different radiation conditions. (b) RL spectra of two kinds of fluorescent layers and the SiO_2 nanosphere coating.

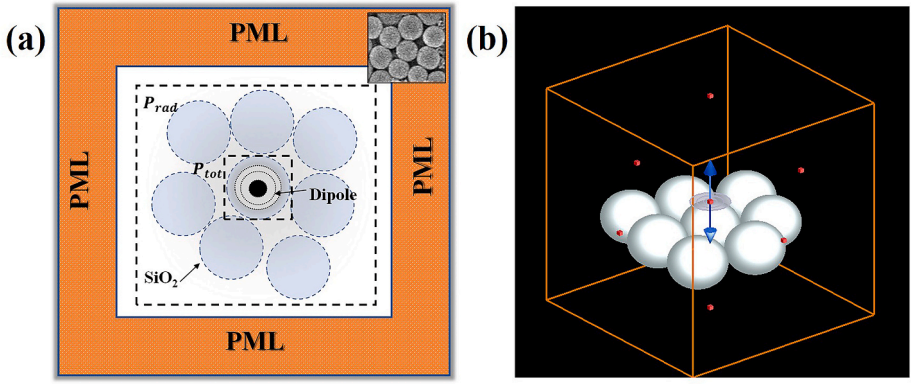

Fig. 7. (a) Model for FDTD simulation and (b) the details of the SiO_2 nanospheres model in 3D space.

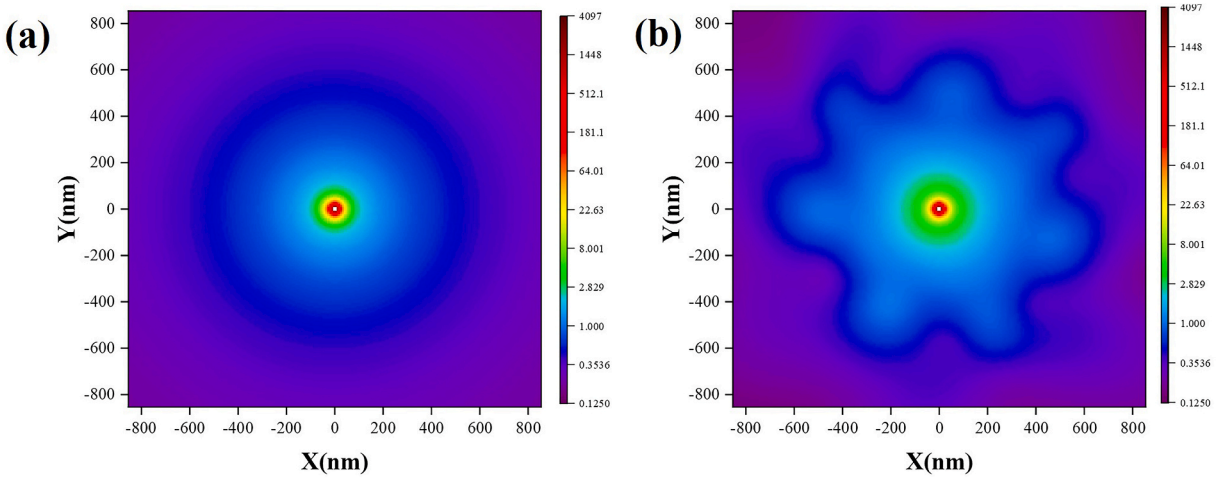

Fig. 8. The electric field intensity distribution of (a) a dipole without SiO_2 and (b) a dipole with SiO_2.

irregular and the electric field intensity is significantly higher at the same position than without adding SiO_2 nanospheres. The change of electric field intensity also affects the excitation rate. When the excitation rate increases, it will affect the spontaneous decay rate and enhance the fluorescence intensity [34–36].

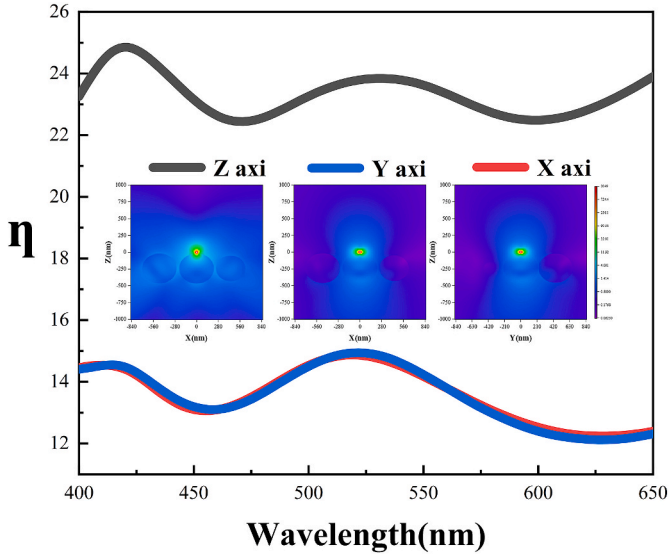

Fig. 9. The influence of different fluorescence emission directions on the enhancement of quantum efficiency and the inset shows the electric field distribution when dipoles emit fluorescence along different directions.

The radioluminescence produced by the phosphor is isotropic and diverges around. Therefore, the change of quantum efficiency and electric field distribution are analyzed when the dipole is emitted along the three directions of the x, y and z axis, as shown in Fig. 9. It can be seen that when the dipole emits fluorescence along the z axis direction, its electric field intensity is much greater than along the x and y axis directions. The reason for this phenomenon is that the fluorescence produced by the dipole interacts with the SiO_2 nanospheres to produce resonance, which changes the field intensity, and improves the quantum efficiency [37–39]. According to the simulation results, when the fluorescence wavelength is 526 nm, the quantum efficiency of the emitter along the z axis increases by 79.2%. But when it emits along the x and y axis, the quantum efficiency only increases by 11.4% and 12.1%. Therefore, when the fluorescence emission direction is perpendicular to the SiO_2 nanospheres, the resonance phenomenon is most obvious, which also corresponds to the electric field distribution. Based on the above study, the method of adding SiO_2 nanosphere coating to the fluorescent layer is an effective way to enhance the radioluminescence intensity without changing the inherent properties of fluorescent material.

3.4. Application of SiO_2 nanosphere coating in radioluminescent nuclear battery

Based on the above-mentioned optical performance study, the electrical performance testing of nuclear batteries through different energy

conversion mechanisms is carried out. According to the different energy conversion mechanisms, the nuclear batteries can be divided into three types. 1) A nuclear battery without a fluorescent layer directly converts X-ray energy into electrical energy. 2) A nuclear battery with a fluorescent layer indirectly converts the energy of X-rays into electrical energy. 3) A nuclear battery decorated with a SiO_2 nanosphere coating on the fluorescent layer indirectly converts X-ray energy into electrical energy. As shown in Fig. 10a–e, the electrical output performance of RLNBs is tested when the voltage of X-ray tube at 40–60 kV, and the tube current of X-ray is kept at 0.8 mA. It can be seen that the electrical output performance of the nuclear battery with fluorescent layer is much greater than that without fluorescent layer. It is because of the strong penetration of X-ray, which can deposit energy in both the fluorescent layer and the PV module, thus making the electrical output performance of the battery stronger. And the electrical output performance of nuclear batteries increases with the X-ray intensity, regardless of the type of energy conversion based.

Fig. 10f shows the variation in output power density among the three kinds of nuclear batteries at different voltages of X-ray tube changes and fits the variation in output power density. It can be seen that adding fluorescent layer can be very effective in improving the output power density of the nuclear battery. The output power density of the nuclear batteries with the additional fluorescent layer can be increased from 0.91 nW/cm^2 to 2.84 nW/cm^2, a 3.12-fold enhancement, when the voltage of X-ray tube is 60 kV. And the output power density of nuclear battery increased to 4.28 nW/cm^2 after using fluorescent layer with SiO_2

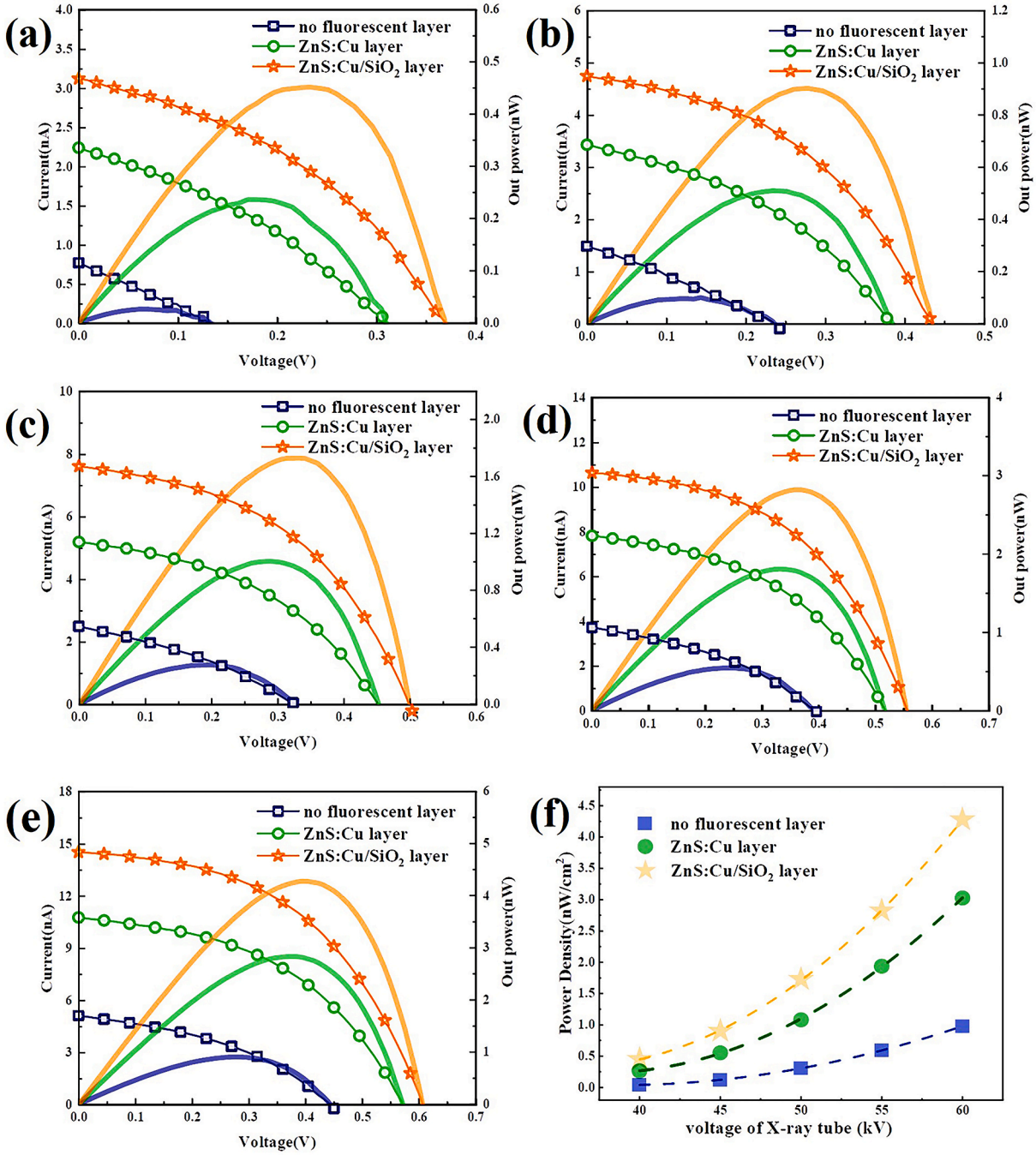

Fig. 10. *I–V* and *P–V* curves of the electrical output of radioluminescent nuclear battery with the current of X-ray tube is 0.8 mA and the voltage of tube is (a) 40 kV, (b) 45 kV, (c) 50 kV, (d) 55 kV, (e) 60 kV. (f) Variation of the output power density of the battery at different voltages of tube.

nanosphere coating, showing 4.7-fold enhancement, due to the enhancement of radioluminescence by the SiO_2 nanospheres coating. In addition, it can be derived from the trend of output power density that with the further increase of X-ray intensity, the difference of output power density between nuclear batteries with fluorescent layer and nuclear battery without fluorescent layer will be greater. The addition of SiO_2 nanosphere coating does not affect the change of this trend and further increases this difference. Therefore, using SiO_2 nanosphere coating to improve the radioluminescence intensity is beneficial to improve the output performance of RLNB.

3.5. Comparing the effect of different fluorescent layers optimization schemes on the batteries

The effects of different fluorescent layer structures on the electrical output performance of RLNBs are compared. As shown in Fig. 11a, four kinds of fluorescent layers are prepared for the comparison in terms of enhancement in RLNB electrical output performance. #1 is a ZnS:Cu fluorescent layer with glass as the substrate, #2 is a ZnS:Cu fluorescent layer with Al as the substrate, #3 is a ZnS:Cu fluorescent layer with glass as the substrate and SiO_2 nanosphere coating added, and #4 is an Al film added behind the fluorescent layer of #1.

The results of the test on electrical output performance are shown in Fig. 11b–e. The electrical output performance of the RLNB can be effectively enhanced by adding Al film or SiO_2 nanosphere coating. The electrical output performance gradually increases with the voltage of X-ray tube in the four kinds fluorescent layer structures. To obtain a good reflection performance of visible light for the Al film used in RLNB #4, we set the thickness at 0.15 mm. The thickness of Al film is thicker than that of SiO_2 nanosphere coating, and it completely covers the fluorescent layer. In RLNB #2, the thickness of Al layer is 2 mm to provide good support for the ZnS:Cu layer. And the Al layer used in RLNB #2 is much thicker than that of RLNB #4, but the electrical output performance of RLNB #4 is higher than that of RLNB #2. It is because the ZnS:Cu phosphor in the fluorescence layer of RLNB #2 is in direct contact with Al and makes a decrease in the radioluminescence intensity produced by the fluorescence layer, due to the phenomenon of fluorescence quenching appearances [40]. And from the test results, under the same radiation conditions, the I_{sc} value of the RLNB with SiO_2 nanosphere coating is higher than that of the RLNB with Al film as the reflector, while the V_{oc} is almost the same probably because the SiO_2 nanosphere coating induces the fluorescence layer to produce a higher radioluminescence intensity. Table 1 lists the I_{sc} and P_{max} values of four kinds of RLNBs when the voltage of X-ray tube is 60 kV and current of X-ray tube is 0.8 mA. It can be seen that the P_{max} value and I_{sc} value increased by 35.68% and 23.32% due to the structure of using Al film. However, under the same condition, the fluorescent layer structure with the addition of SiO_2 nanosphere coating results in a greater increase in RLNB output performance, the P_{max} value increase of up to 51.59% and the I_{sc} value to 35.63%. The results show that the design and optimization of the fluorescence layer structures can indeed enhance the electrical output performance and the SiO_2 nanosphere coating can also enhance the radioluminescence intensity without changing the other properties of the material.

4. Conclusion

In this work, we propose a method for enhancing the radioluminescence intensity without changing the structure and properties of the ZnS:Cu phosphor. The specific approach is to gravitational deposition method the SiO_2 nanosphere coating on the substrate, and then prepare the ZnS:Cu fluorescent layer by spin-coating method. The increase in the radioluminescence intensity of the fluorescent layer by 62.32% is attributed to the enhancement of the quantum efficiency of

Table 1
The I_{sc} and P_{max} value of the radioluminescent nuclear battery at the voltage of X-ray tube is 60 kV and the current of X-ray tube is 0.8 mA.

Sample	RLNB #1	RLNB #2	RLNB #3	RLNB #4
I_{sc} (nA)	10.72	12.77	14.54	13.22
P_{max} (nW)	2.83	3.67	4.29	3.84

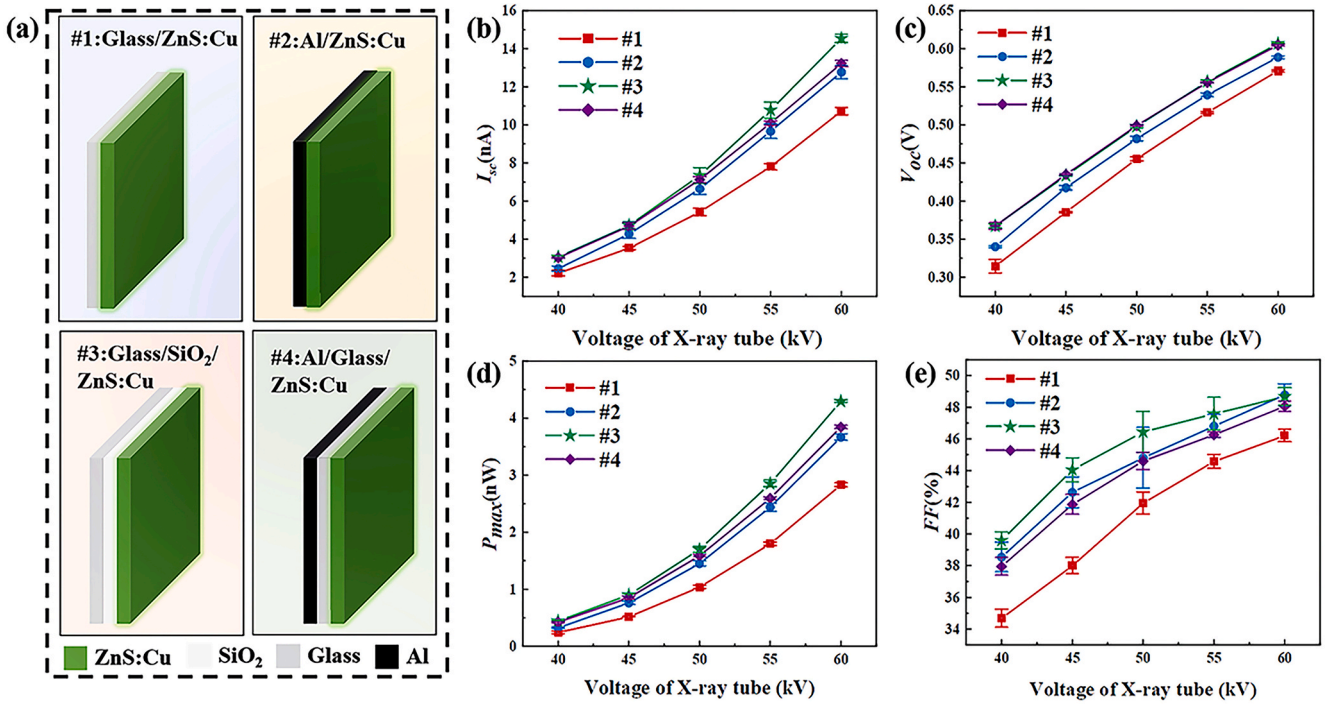

Fig. 11. (a) Four different structures of ZnS:Cu fluorescent layers. Electrical properties of the radioluminescent nuclear battery with different fluorescent layers under different voltage of the X-ray tube, (b) short circuit current I_{sc}, (c) open circuit voltage V_{oc}, (d) maximum output power P_{max}, and (e) fill factor *FF*.

the ZnS:Cu phosphor by the SiO_2 nanospheres. And the method can increase the maximum output power of the radioluminescent nuclear battery by 51.59%, when X-ray is used as the source of radiation. And the results from a series of test data indicate that the radioluminescent nuclear battery's output performance increases as the X-ray intensity increases and the SiO_2 nanosphere coating can further improve the performance amplification. Moreover, the electrical output performance of the radioluminescent nuclear battery can also be improved by changing the structure of the fluorescent layer. This method of our work has more advantages compared with other fluorescent layer structure design methods. The method of adding SiO_2 nanosphere coating to enhance the radioluminescence of ZnS:Cu is not only of great significance to increasing electrical performance output of the radioluminescent nuclear battery, but also helpful to the applications in other areas, such as lighting devices, optoelectronic devices and detectors.

Credit author statement

Yuhang He: Conceptualization, Methodology, Formal analysis, Investigation, Writing-Original draft, Writing–Review & Editing; **Zhiheng Xu:** Validation, Data curation, Formal analysis, Writing-Reviewing and Editing, Funding acquisition, Supervision; **Hongyu Wang:** Visualization; **Mingxin Bian:** Investigation; **Yunpeng Liu:** Funding acquisition, Supervision; **Xiaobin Tang:** Writing-Reviewing and Editing, Supervision, Project administration.

Declaration of competing interest

The authors declare that they have no known competing financial interests or personal relationships that could have appeared to influence the work reported in this paper.

Data availability

Data will be made available on request.

Acknowledgements

This work is supported by the National Natural Science Foundation of China (Grant No. 12005101), the Natural Science Foundation of Jiangsu Province (Grant No. BK20201288), China Postdoctoral Science Foundation (Grant No. 2022M711613) and the Excellent Postdoctoral Program of Jiangsu Province (Grant No. 2022ZB235).

References

[1] A. Krasnov, S. Legotin, K. Kuzmina, N. Ershova, B. Rogozev, A nuclear battery based on silicon p-i-n structures with electroplating ^{63}Ni layer, Nucl. Eng. Technol. 51 (2019) 1978–1982.
[2] X. Wang, Y. Han, J. Zhang, Z. Li, T. Li, X. Zhao, Y. Wu, The design of a direct charge nuclear battery with high energy conversion efficiency, Appl. Radiat. Isot. 148 (2019) 147–151.
[3] T. Jiang, Z. Xu, C. Meng, Y. Liu, X. Tang, In-depth analysis of the internal energy conversion of nuclear batteries and radiation degradation of key materials, Energy Technol. 8 (2020), 2000667.
[4] Z. Xu, Z. Jin, X. Tang, Y. Liu, X. Guo, C. Peng, H. Wang, Designing performance enhanced nuclear battery based on the Cd-109 radioactive source, Int. J. Energy Res. 44 (2020) 508–517.
[5] Z. Xu, Y. Liu, X. Tang, Radioluminescent nuclear battery Technology development for space exploration, Adv. Astronaut. Sci. Technol. 3 (2020) 125–131.
[6] S. Xue, C. Tan, P. Kandlakunta, I. Oksuz, V. Hlinka, L.R. Cao, Methods for improving the power conversion efficiency of nuclear-voltaic batteries, Nucl. Instruments Methods Phys. Res. Sect. A Accel. Spectrometers, Detect. Assoc. Equip. 927 (2019) 133–139.
[7] Y. Lei, Y. Yang, G. Li, Y. Liu, J. Xu, X. Xiong, S. Luo, T. Peng, Demonstration and aging test of a radiation resistant strontium-90 betavoltaic mechanism, Appl. Phys. Lett. 116 (2020), 153901.
[8] A.B. Phatangare, S.V. Bhoraskar, S.S. Dahiwale, S.D. Dhole, V.N. Bhoraskar, Novel nuclear batteries based on radioluminescence, Energy Technol. 10 (2022), 2200285.
[9] S. Xue, C. Tan, P. Kandlakunta, I. Oksuz, V. Hlinka, L.R. Cao, Methods for improving the power conversion efficiency of nuclear-voltaic batteries, Nucl. Instruments Methods Phys. Res. Sect. A Accel. Spectrometers, Detect. Assoc. Equip. 927 (2019) 133–139.
[10] C. Zhao, J. Ren, L. Lei, F. Liao, X. Shi, D. Zhou, K. Liu, Y. Zhao, Tenfold efficiency improvement of x-ray radioluminescent batteries basing on GAGG:Ce single crystal scintillators, Appl. Phys. Lett. 119 (2021), 223901.
[11] W. Chen, X. Tang, Y. Liu, Z. Xu, Y. Zicheng, Z. Zhang, K. Liu, Radioluminescent nuclear battery containing $CsPbBr_3$ quantum dots: Application of a novel wave-shifting agent, Int. J. Energy Res. 43 (2019) 4520–4533.
[12] X. Tang, Z. Xu, Y. Liu, M. Liu, H. Wang, D. Chen, Physical parameters of phosphor layers and their effects on the device properties of beta-radioluminescent nuclear batteries, Energy Technol. 3 (2015) 1121–1129.
[13] Z. Xu, Y. Liu, Z. Zhang, W. Chen, Z. Yuan, K. Liu, X. Tang, Enhanced radioluminescent nuclear battery by optimizing structural design of the phosphor layer, Int. J. Energy Res. 42 (2018) 1729–1737.
[14] L. Hong, X. Bin Tang, Z.H. Xu, Y.P. Liu, D. Chen, Radioluminescent nuclear batteries with different phosphor layers, Nucl. Instrum. Methods Phys. Res. Sect. B Beam Interact. Mater. Atoms 338 (2014) 112–118.
[15] J. Russo, M. Litz, W. Ray, B. Smith, R. Moyers, A radioluminescent nuclear battery using volumetric configuration: ^{63}Ni solution/ZnS:Cu,Al/InGaP, Appl. Radiat. Isot. 130 (2017) 66–74.
[16] Z. Xu, X. Tang, Y. Liu, Z. Zhang, W. Chen, K. Liu, Z. Yuan, $CsPbBr_3$ quantum dot films with high luminescence efficiency and irradiation stability for radioluminescent nuclear battery application, ACS Appl. Mater. Interfaces 11 (2019) 14191–14199.
[17] D. Yang, Z. Xu, C. Gong, L. Su, X. Li, X. Tang, D. Geng, C. Meng, F. Xu, H. Zeng, Armor-like passivated $CsPbBr_3$ quantum dots: boosted stability with hand-in-hand ligands and enhanced performance of nuclear batteries, J. Mater. Chem. A. 9 (2021) 8772–8781.
[18] X. Li, J. Chen, D. Yang, X. Chen, D. Geng, L. Jiang, Y. Wu, C. Meng, H. Zeng, Mn^{2+} induced significant improvement and robust stability of radioluminescence in $Cs_3Cu_2I_5$ for high-performance nuclear battery, Nat. Commun. 12 (2021) 3879.
[19] C.K. Rastogi, R.K. Mishra, S. Chirauri, K.R. Rao, R.K. Vatsa, R.M. Kadam, V. Sudarsan, Comparative study on photo and electroluminescence properties of Cu-doped ZnS, Phys. B Condens. Matter 640 (2022), 414054.
[20] K. Hoang, C. Latouche, S. Jobic, Defect energy levels and persistent luminescence in Cu-doped ZnS, Comput. Mater. Sci. 163 (2019) 63–67.
[21] K. Priya, V.K. Ashith, G.K. Rao, G. Sanjeev, A comparative study of structural, optical and electrical properties of ZnS thin films obtained by thermal evaporation and SILAR techniques, Ceram. Int. 43 (2017) 10487–10493.
[22] G. Saatsakis, N. Kalyvas, C. Michail, K. Ninos, A. Bakas, C. Fountzoula, I. Sianoudis, G.E. Karpetas, G. Fountos, I. Kandarakis, I. Valais, G. Panayiotakis, Optical characteristics of ZnCuInS/ZnS (Core/Shell) nanocrystal flexible films under X-ray excitation, Crystals 9 (2019) 343.
[23] A. Jesu Jebathew, M. Karunakaran, R. Ade, J.S. Ponraj, V. Ganesh, R.K. Manavalan, Y. Bitla, I.S. Yahia, H. Algarni, Highly sensitive hexagonal-shaped ZnS–Cu thin films for photo-detector applications, J. Mater. Sci. Mater. Electron. 33 (2022) 2192–2203.
[24] K. Priya, G.K. Rao, V.K. Ashith, G. Sanjeev, V.P. Verma, V.C. Petwal, J. Dwivedi, The effect of 8 MeV electron beam irradiation on the structural, optical and photoluminescence properties of ZnS thin films, Ceram. Int. 45 (2019) 2576–2583.
[25] T. Jiang, Z. Xu, X. Tang, Z. Yuan, H. Wang, M. Bian, Comparison and study of the preparation methods for phosphor layer in nuclear battery, Int. J. Energy Res. 45 (2021) 11712–11720.
[26] Z.R. Zhang, Y.P. Liu, X. Bin Tang, Z.H. Xu, Z.C. Yuan, K. Liu, W. Chen, GaAs low-energy X-ray radioluminescence nuclear battery, Nucl. Instrum. Methods Phys. Res. Sect. B Beam Interact. Mater. Atoms 415 (2018) 9–16.
[27] H. Alhalaby, H. Zaraket, M. Principe, Enhanced photoluminescence with dielectric nanostructures: a review, Results Opt 3 (2021), 100073.
[28] Y. Yan, J. Liu, C. Xing, Q. Wang, Y. Zeng, Y. Zhao, Y. Jiang, Parametric study on photoluminescence enhancement of high-quality zinc oxide single-crystal capping with dielectric microsphere array, Appl. Opt. 57 (2018) 7740–7749.
[29] A. Barreda, S. Hell, M.A. Weissflog, A. Minovich, T. Pertsch, I. Staude, Metal, dielectric and hybrid nanoantennas for enhancing the emission of single quantum dots: a comparative study, J. Quant. Spectrosc. Radiat. Transf. 276 (2021), 107900.
[30] A. Devilez, B. Stout, N. Bonod, Compact metallo-dielectric optical antenna for ultra directional and enhanced radiative emission, ACS Nano 4 (2010) 3390–3396.
[31] L. He, L. Yang, B. Liu, J. Zhang, C. Zhang, S. Liu, S. Chen, J.A. Zapien, K.A. Alamry, A.M. Asiri, K. Zhang, S. Wang, One-pot synthesis of color-tunable copper doped zinc sulfide quantum dots for solid-state lighting devices, J. Alloys Compd. 787 (2019) 537–542.
[32] M. Ayvacıklı, A. Canimoglu, Y. Karabulut, Z. Kotan, L.K.S. Herval, M.P.F. de Godoy, Y. Galvão Gobato, M. Henini, N. Can, Radioluminescence and photoluminescence characterization of Eu and Tb doped barium stannate phosphor ceramics, J. Alloys Compd. 590 (2014) 417–423.
[33] S. Yuan, X. Zhang, W. Cao, Y. Sheng, C. Liu, L. Yu, Y. Di, Z. Chen, L. Dong, Z. Gan, Fluorescence enhancement of perovskite nanocrystals using photonic crystals, J. Mater. Chem. C 9 (2021) 908–915.
[34] A.N. Poddubny, P.A. Belov, Y.S. Kivshar, Spontaneous radiation of a finite-size dipole emitter in hyperbolic media, Phys. Rev. A - At. Mol. Opt. Phys. 84 (2011) 1–6.
[35] X. Ma, H. Tan, T. Kipp, A. Mews, Fluorescence enhancement, blinking suppression, and gray states of individual semiconductor nanocrystals close to gold nanoparticles, Nano Lett. 10 (2010) 4166–4174.
[36] S. Sun, L. Wu, P. Bai, C.E. Png, Fluorescence enhancement in visible light: Dielectric or noble metal? Phys. Chem. Chem. Phys. 18 (2016) 19324–19335.

[37] R. Regmi, J. Berthelot, P.M. Winkler, M. Mivelle, J. Proust, F. Bedu, I. Ozerov, T. Begou, J. Lumeau, H. Rigneault, M.F. García-Parajó, S. Bidault, J. Wenger, N. Bonod, All-Dielectric silicon nanogap antennas to enhance the fluorescence of single molecules, Nano Lett. 16 (2016) 5143–5151.

[38] M.H. Chowdhury, J. Pond, S.K. Gray, J.R. Lakowicz, Systematic computational study of the effect of silver nanoparticle dimers on the coupled emission from nearby fluorophores, J. Phys. Chem. C 112 (2008) 11236–11249.

[39] Z.H. Chen, H. Shi, Y. Wang, Y. Yang, S. Liu, H. Ye, Sharp convex gold grooves for fluorescence enhancement in micro/nano fluidic biosensing, J. Mater. Chem. B. 5 (2017) 8839–8844.

[40] I.J. Kim, Y. Xu, K.H. Nam, Spectroscopic analysis of Fe ion-induced fluorescence quenching of the green fluorescent protein ZsGreen, J. Fluoresc. 31 (2021) 307–314.